*Protein & Cell*, 2026, **17**, 157–162
https://doi.org/10.1093/procel/pwaf078
Advance access publication 08 October 2025
Letter

Protein & Cell

# Letter

## Pleural cavity macrophages promote lung tumor establishment through tissue invasion

Zhenqian Zhang[1,‡], Hengwei Jin[2,‡], Zhicong Liu[3,‡], Mengyang Shi[2], Mingjun Zhang[2], Wenjuan Pu[2], Jie Li[2], Xuekun Li[3], Daqing Ma[4,5,*], Qiang Shu[3,*], Bin Zhou[1,2,6,*]

[1]Key Laboratory of Systems Health Science of Zhejiang Province, School of Life Science, Hangzhou Institute for Advanced Study, Hangzhou 310024; University of Chinese Academy of Sciences, China
[2]CAS CEMCS-CUHK Joint Laboratory, New Cornerstone Science Laboratory, Key Laboratory of Multi-Cell Systems, Shanghai Institute of Biochemistry and Cell Biology, Center for Excellence in Molecular Cell Science, Chinese Academy of Sciences, University of Chinese Academy of Sciences, Shanghai 200031, China
[3]Department of Pediatric Cardiac Surgery, Children's Hospital, Zhejiang University School of Medicine, National Clinical Research Center for Child Health, Hangzhou 310000, China
[4]Perioperative and Systems Medicine Laboratory and Department of Anesthesiology, Children's Hospital, Zhejiang University School of Medicine, National Clinical Research Centre for Child Health, Hangzhou 310000, China
[5]Division of Anaesthetics, Pain Medicine and Intensive Care, Department of Surgery and Cancer, Faculty of Medicine, Chelsea and Westminster Hospital, Imperial College London, London SW10 9NH, United Kingdom
[6]School of Life Science and Technology, ShanghaiTech University, Shanghai 201210, China

[‡]= equal contribution.
*Correspondence: d.ma@imperial.ac.uk (D. Ma), shuqiang@zju.edu.cn (Q. Shu), zhoubin@sibs.ac.cn (B. Zhou)

**Dear Editor,**

Preclinical studies have elegantly demonstrated that distinct populations of cavity-resident macrophages in the peritoneal and pleural spaces are ontogenically, transcriptionally, and functionally related (Buechler et al., 2019). Notably, these cavities are recognized as immunosuppressive environments that commonly facilitate cancer progression (Donnenberg et al., 2019; Morano et al., 2016; Porcel et al., 2015). Cavity-resident macrophages mediate a physiological checkpoint that limited anti-tumor activity at these cancer sites (Chow et al., 2021). Previous genetic lineage tracing has shown that, post-injury, cavity macrophages tend to accumulate on the surfaces of visceral organs, including the lungs (Jin et al., 2021, 2022), rather than deeply infiltrating the parenchyma (Deniset et al., 2019; Wang and Kubes, 2016). However, it remains unclear whether, in the context of tumors, these cavity macrophages penetrate into the lung parenchyma and promote tumor growth. Utilizing dual recombinase-mediated genetic lineage tracing, we observed the infiltration of cavity macrophages into lung tumor metastases. Furthermore, genetic ablation or sequestration of these cavity macrophages significantly reduced tumor growth in the lungs. This observation underscores the crucial role that cavity macrophages play in supporting tumorigenic processes, suggesting that targeting these cells may represent a viable therapeutic strategy for mitigating lung tumor progression.

To simulate the recruitment and invasion of *GATA6*$^+$ cavity macrophages in the B16F10 melanoma lung metastasis mouse model, we employed the *Gata6-rox-Stop-rox-CreER* (*Gata6-iCreER*) knock-in mice. In this model, Dre-*rox* removes a *rox*-flanked Stop sequence, yielding a *Gata6-CreER* allele. We crossed these mice with *CD45-Dre* (Jin *et al.*, 2021) and *R26-tdTomato* (*R26-tdT*) (Madisen et al., 2010) mice to enable specific lineage tracing of pleural cavity macrophages (Fig. 1A). CD45 markers can distinguish macrophages (CD45$^+$) from CD45$^-$ organ cells like hepatocytes, cardiomyocytes, etc. The *GATA6* marker can differentiate cavity macrophages (*GATA6*$^+$) from recruited monocytes OR tissue-resident macrophages (*GATA6*$^-$). Therefore, theoretically, double-positive cells (CD45$^+$*GATA6*$^+$) would be cavity macrophages, distinct from tissue-resident macrophages, monocytes, and other cell lineages such as hepatocytes, cardiomyocytes, or lung epithelial cells (Fig. 1B). For proof of principle, we crossed *CD45-Dre*; *Gata6-iCreER* mice with *R26-tdT* mice and analyzed the labeling of monocytes and macrophages 2 weeks after tamoxifen (Tam) treatment (Fig. 1C). Immunofluorescent (IF) staining revealed that the majority of pleural macrophages expressing *GATA6* and F4/80 were

Accepted 06 August 2025

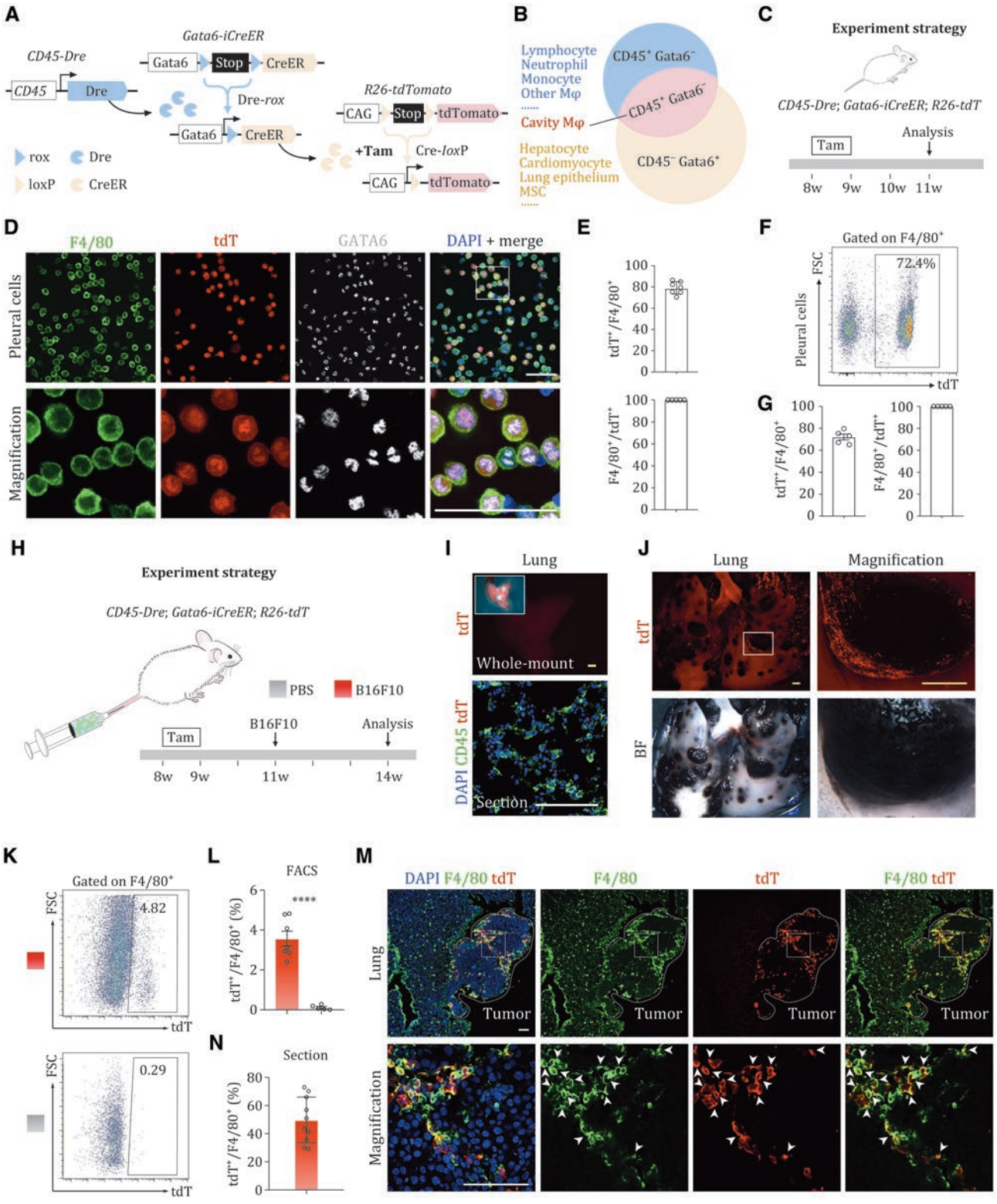


**Figure 1. Pleural cavity macrophages invade into lung tumors.** (A) Schematic figure showing *CD45-Dre* mediates Stop cassette removal from *Gata6-iCreER* and places *CreER* directly under the Gata6 promoter. After tamoxifen (Tam), Cre-loxP recombination labels cells by tdT. (B) Intersectional genetics marks CD45$^+$GATA6$^+$ cells as tdT$^+$. (C) Schematic figure showing experimental design using cavity macrophage tracing tool *CD45-Dre*; *Gata6-iCreER*; *R26-tdT*. (D) Immunostaining for tdT, GATA6, and F4/80 on dissociated cells from the pleural cavity. Boxed regions are magnified. Scale bars, 50 μm. (E) Quantification of the proportion of F4/80$^+$ macrophages that express tdT, and the proportion of tdT$^+$ cells that express F4/80. Data are the mean ± SD; $n \geq 5$. (F) Flow cytometric analysis of the percentage of tdT$^+$ cells in macrophages from the pleural cavity with Tam. (G) Quantification of the percentage of tdT$^+$ cells in F4/80$^+$ macrophages. Data are the mean ± SD; $n = 5$ mice per group. (H) A schematic showing the experimental strategy. (I) Whole-mount fluorescence images and immunostaining for CD45 and tdT show no resident tdT$^+$ macrophages in the lung. Scale bar: 1mm (upper panel), 100μm (lower panel). (J) Whole-mount bright-field and fluorescence images of lungs from mice inoculated with B16F10 cells. Scale bar: 1mm. (K and L) Flow

tdT$^+$ in Tam-treated *CD45-Dre*; *Gata6-iCreER*; *R26-tdT* mice (Fig. 1D). Quantitative analysis revealed that all tdT$^+$ cells expressed F4/80, and 79.2% of F4/80$^+$ cells were positive for tdT (Fig. 1E). Virtually fluorescence-activated cell sorter (FACS) analysis showed all tdT$^+$ pleural cells (>99.5%) were CD11b$^+$F4/80$^+$ (Fig. 1F and 1G), indicating high specificity of *CD45-Dre*; *Gata6-iCreER* for labeling cavity macrophages. Adult *CD45-Dre*; *Gata6-iCreER*; *R26-tdT* mice (8 weeks old) were administered Tam for 1 week to induce gene recombination. Two weeks after the final Tam treatment, mice were intravenously injected with $2 \times 10^5$ B16F10 melanoma cells *via* the tail vein to establish a lung metastasis model (Fig. 1H). In lungs collected from mice treated with phosphate-buffered saline (PBS), we did not detect tdT expression in CD45$^+$ cells, excluding ectopic labeling of resident macrophages or other hematopoietic cell lineages in visceral organs (Fig. 1I). Notably, whole-mount fluorescent imaging revealed prominent tdT$^+$ signals covering the tumor surface (Fig. 1J). Flow cytometric analysis showed the presence of infiltrated pleural cavity macrophages in the melanoma (Fig. 1K). Quantification data indicated that tdT$^+$ macrophages constituted approximately 3.6% of all lung macrophages in the mice inoculated with B16F10 melanoma cells, compared to minimal tdT$^+$ macrophages detected in control lungs without tumor inoculation (Fig. 1L). Immunostaining for tdT and F4/80 on lung sections revealed an accumulation of tdT$^+$ cavity macrophages within tumors at the lung periphery (Fig. 1M). Importantly, pleural cavity macrophages did not infiltrate the normal (non-tumor) alveolar region or the adventitial space, suggesting their specific involvement in tumors. Quantification of the immunofluorescence-stained images of lung edge tumors showed that tdT$^+$ cells constituted about 50% of the macrophages infiltrating the tumors (Fig. 1N), indicating a significant involvement of pleural cavity macrophages in the tumor growth and suggesting a crucial role in shaping the tumor microenvironment. To further investigate whether pleural cavity macrophages are able to infiltrate other types of tumors, we employed two additional tumor cell lines, the mouse hepatoma cell line Hepa1-6 (Hepa1-6) and Lewis lung Carcinoma (LLC) (Fig. S1), both of which are capable of forming lung metastases. Three weeks after tumor cell injection, whole-lung fluorescence imaging of *CD45-Dre*; *Gata6-iCreER*; *R26-tdT* mice revealed a strong accumulation of red fluorescent signals over the tumor regions (Fig. S1A, S1B, S1E, and S1F). This pattern was consistently observed in both Hepa1-6 and LLC lung metastasis models. Further analysis of lung sections by immunofluorescence staining for F4/80 and tdT revealed that pleural cavity macrophages contributed to approximately half of the macrophage population within the tumor regions (Fig. S1C, S1D, S1G, and S1H). These findings are consistent with those observed in the B16F10 melanoma lung metastasis model, suggesting a generalizable role of pleural cavity macrophages across different tumor types.

To specifically elucidate the role of *GATA6*$^+$ cavity macrophages in influencing tumor growth, we aimed to selectively ablate these cells during the progression of tumor development. We engineered a *Gata6-RSR-tdT-DTR* knock-in mouse line, wherein a genetic construct driven by the *Gata6* promoter enables the expression of both the diphtheria toxin receptor (DTR) and tdT following the excision of a *rox-Stop-rox* sequence in Dre-expressing cells (Fig. 2A). In the *CD45-Dre*; *Gata6-RSR-tdT-DTR* mice, Dre-*rox* recombination specifically removes the RSR cassette in CD45$^+$ cell lineages, resulting in the exclusive expression of tdT and DTR in *GATA6*$^+$ pleural or peritoneal cavity macrophages (Fig. 2A and 2B). To assess the efficiency of tdT$^+$ cell ablation, adult mice were treated with either diphtheria toxin (DT) or PBS (Fig. 2B). Immunostaining of isolated cavity cells demonstrated the colocalization of tdT and DTR expression within peritoneal and pleural cavity macrophages (Fig. 2C), confirming the successful creation of a cavity macrophage-specific DTR expression system. Additional IF staining and flow cytometric analysis consistently showed that the majority of pleural and peritoneal macrophages expressing *GATA6* and F4/80 were tdT positive (Figs. 2D, S2A and S2B). In DT-treated *Cd45-Dre*; *Gata6-RSR-tdT-DTR* mice, tdT$^+$ cavity macrophages were markedly reduced within 3 days, as confirmed by immunostaining for tdT, compared with PBS controls (Fig. 2D and 2E). Flow cytometric analysis further confirmed a significant reduction in the percentage of tdT$^+$ macrophages among CD45$^+$ peritoneal or pleural cells (Fig. 2F and 2G). Considering the concern regarding the potential resistance of immune cells to DT-mediated depletion, we sought to evaluate the duration of DT-induced depletion of cavity macrophages. We accordingly evaluated the numbers of pleural and peritoneal cavity macrophages 3 weeks after DT administration, ensuring consistency in the experimental timeline (Fig. S2C). Flow cytometry analysis demonstrated that, 3 weeks after DT treatment, the proportions of pleural and peritoneal cavity macrophages remained significantly lower than those in the PBS control group, indicating a sustained depletion effect (Fig. S2D and S2E). Moreover, an absence of tdT expression in *GATA6*$^+$ cells across all examined visceral organs from *CD45-Dre*; *Gata6-RSR-tdT-DTR* mice confirmed that there was no ectopic labeling of tissue-resident macrophages or hematopoietic cell lineages in these organs (Fig. S2F and S2G). Overall, the

cytometric analysis of the percentage of F4/80$^+$ macrophages expressing tdT. Data are the mean ± SD; $n = 5$ mice per group. (M) Immunostaining for tdT and F4/80 on lung sections. Scale bar: 100μm. (N) Quantification of the percentage of F4/80$^+$ macrophages expressing tdT in tumors located at the lung periphery. Data are the mean ± SD; $n = 5$ mice per group.

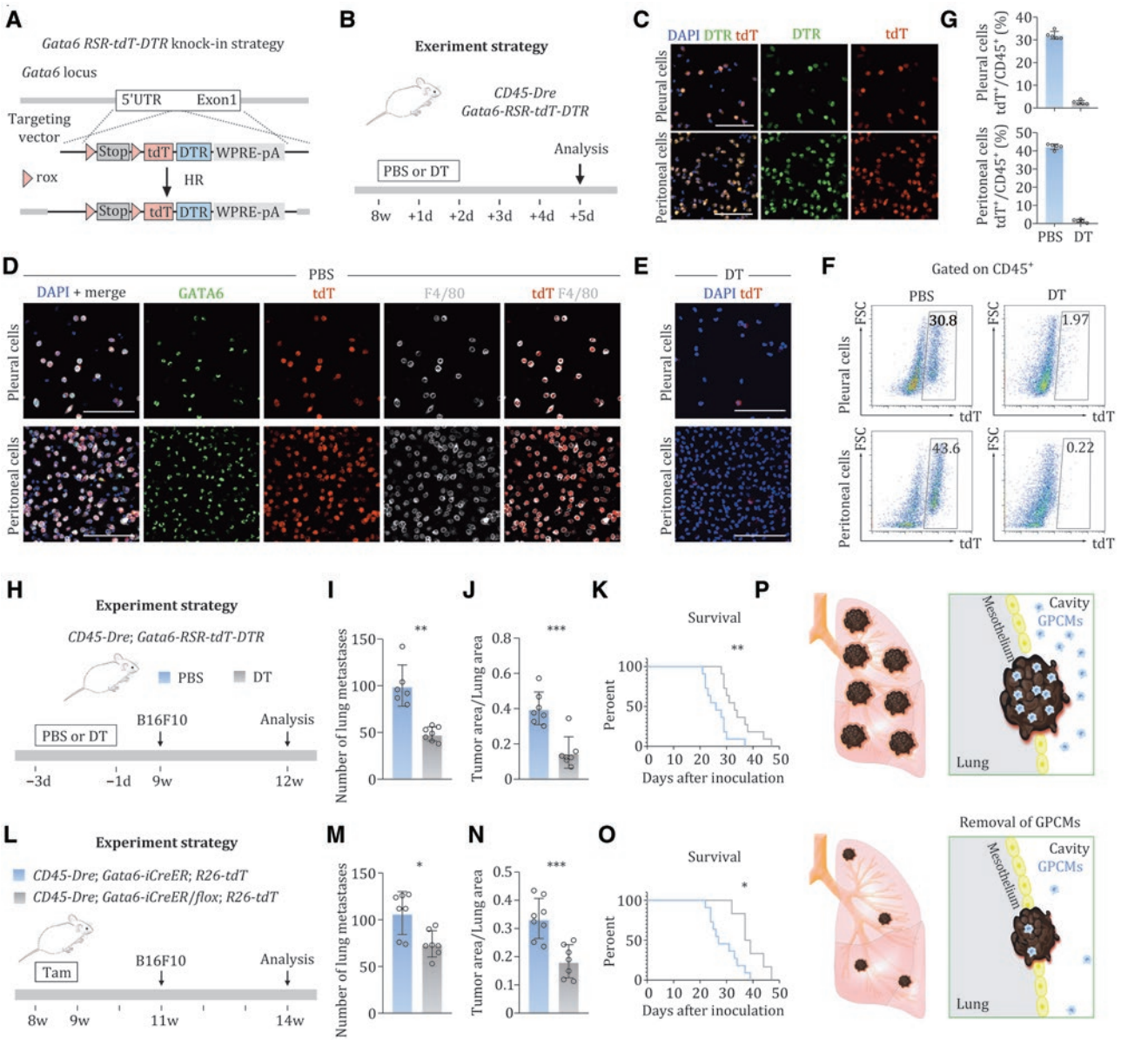


**Figure 2. The function of pleural cavity macrophages in lung tumors.** (A) A schematic showing the knock-in strategy for the generation of the *Gata6-RSR-tdT-DTR* allele. (B) A schematic showing the experimental strategy. (C) Immunostaining for tdT and DTR on dissociated cells from the pleural and peritoneal cavity. (D) Immunostaining for GATA6, tdT, and F4/80 on the dissociated cells. (E) Immunostaining for tdT on dissociated cells from mice treated with DT. (F and G) Flow cytometric analysis of the percentage of tdT$^+$ cells in immune cells from the pleural and peritoneal cavities of mice treated with PBS or DT. (H) A schematic showing genetic ablation of cavity macrophages. (I) Quantification of the number of B16F10 lung metastases. Data are the mean ± SD; $n=5$ mice per group. (J) Quantification of the ratio of tumor-covered area to total lung area. Data are the mean ± SD; $n=5$ mice per group. (K) Kaplan–Meier plot illustrating the survival rates of mice in the study. $n=5$ mice per group. (L) A schematic figure showing the experimental design of *Gata6* deletion in cavity macrophages. (M) Quantification of the number of B16F10 lung metastases. Data are the mean ± SD; $n=5$ mice per group. (N) Quantification of the ratio of tumor-covered area to total lung area. Data are the mean ± SD; $n=5$ mice per group. (O) Kaplan–Meier plot illustrating the survival rates of mice in the study. $n=5$ mice per group. (P) Cartoon image showing ablation of Gata6$^+$ pleural cavity macrophages (GPCMs) significantly reduces tumors in the lung. Scale bar: 100 μm.

development of the *CD45-Dre*; *Gata6-RSR-tdT-DTR* mouse line facilitates specific and efficient ablation of endogenous cavity macrophages.

We next examined the role of pleural cavity macrophages in the B16F10 melanoma lung metastasis mouse model by treating *CD45-Dre*; *Gata6-RSR-tdT-DTR* mice with DT or PBS (Fig. 2H). DT-treated *CD45-Dre*; *Gata6-RSR-tdT-DTR* mice exhibited significant resistance to B16F10 cell metastasis in the lungs compared to PBS-treated controls (Fig. 2I). By day 21, whole-mount bright field imaging showed significantly fewer metastatic melanoma lesions on the lung surface in DT-treated mice (Figs. 2J, S3A and S3B). Additionally, Masson-Fontana staining revealed a marked decrease in the area of lung

metastasis in DT-treated *CD45-Dre*; *Gata6-RSR-tdT-DTR* mice compared to the control group (Fig. S3A and S3B). These mice also demonstrated an extended survival rate (Fig. 2K). Given that *GATA6* is a key transcription factor influencing the survival and proliferation of peritoneal macrophages (Rosas et al., 2014), we proceeded to knock out *Gata6* in cavity macrophages. We crossed *CD45-Dre*; *Gata6-iCreER*; *R26-tdT* mice with *Gata6-flox* mice (Sodhi et al., 2006), and treated the offspring, *CD45-Dre*; *Gata6-iCreER/flox*; *R26-tdT* mice, with Tam between weeks 8 and 9 of age to simultaneously label cavity macrophages and delete *Gata6* (Fig. 2L). Two weeks later, these mice were inoculated with B16F10 melanoma cells. Littermate *CD45-Dre*; *Gata6-iCreER*; *R26-tdT* mice served as control. To examine how *Gata6* gene knockout affects the number of pleural cavity macrophages, we performed flow cytometric analysis to quantify the absolute numbers of pleural cavity macrophages, peritoneal macrophages, and tumor-infiltrating pleural macrophages. We found that specific deletion of *Gata6* led to a marked reduction in the number of cavity macrophages in the peritoneal and pleural spaces, as well as within the tumor (Fig. S3C and S3D). Whole-mount bright field images and Masson-Fontana staining of lungs showed that a significant reduction of tumor numbers in cavity macrophage-specific *Gata6* knockout mice compared to control mice (Fig. 2M, 2N, S3E and S3F). Additionally, the survival of *CD45-Dre*; *Gata6-iCreER/flox*; *R26-tdT* mice was notably increased compared to the control mice (Fig. 2O). Taken together, the ablation of cavity macrophages or knockout of *Gata6* in these cells resulted in reduced metastasis, decreased tumor burden, and notably extended survival rates.

To assess the role of pleural cavity macrophages in established tumors, we initiated DT treatment 2 weeks after intravenous inoculation of melanoma cells, allowing sufficient time for tumor establishment, and performed analysis in the third week (Fig. S4A). Whole-mount bright field imaging revealed a trend of decreased lung metastases in DT-treated mice compared to PBS controls, but without statistical significance (Fig. S4B–D). Further Masson-Fontana staining revealed a slight decrease in tumor area, and the survival curve suggested a potential improvement in survival following DT treatment (Fig. S4B–F). Based on the above experimental results, DT-mediated depletion of pleural cavity macrophages after tumor establishment showed limited efficacy in suppressing tumor progression. These findings suggest that pleural cavity macrophages play a pivotal role during the early establishment phase of lung tumors, facilitating initial tumor growth and microenvironmental conditioning. Their influence appears to diminish but may still persist to a limited extent once tumors are more established. Therefore, targeting these cells may be most effective at early stages of tumor development. To investigate the role of cavity macrophages in the development of primary tumors derived from inoculated melanoma cells, we directly injected B16F10-Luc cells into the pleural cavity, where they formed primary tumors (Fig. S4G). This model allowed us to explore the specific functions of pleural cavity macrophages in the local tumor microenvironment. Bioluminescence imaging showed that depletion of pleural cavity macrophages markedly inhibited the growth rate of primary tumors (Fig. S4H and S4I). Taken together, these results indicate that pleural cavity macrophages promote the growth of both metastatic and primary melanoma tumors.

To explore the mechanisms behind the role of cavity macrophages in tumorigenic processes, we included a comprehensive immune profiling analysis to investigate how depletion of cavity macrophages contributes to reduced tumor growth in the B16F10 melanoma lung metastasis model. Flow cytometry was used to analyze changes in the proportions of immune cells in lung tumors and pleural cells following the depletion of cavity macrophages (Fig. S5A). We examined the changes in the proportions of lymphoid and myeloid cells separately. For myeloid cells, monocytes were identified as $CD11b^+LY6G^-LY6C^+$, neutrophils as $CD11b^+LY6G^+$, and macrophages as $F4/80^+$ cells. For lymphoid cells, T cells were identified as $CD3^+$, B cells as $CD19^+$, and natural killer (NK) cells as $CD3^-CD19^-NK1.1^+$ cells. Compared with mice not treated with DT, we found no significant changes in the proportions of neutrophils and macrophages among myeloid cells in lung tumors (Fig. S5B). However, the proportion of monocytes was increased, which we speculate may be due to a compensatory response in which monocytes capable of differentiating into macrophages partially compensate for the loss of cavity macrophages. Among lymphoid cells, we observed an increased proportion of T cells, a decreased proportion of B cells, and no significant change in the proportion of NK cells (Fig. S5B). We also analyzed cells from the pleural cavity. In DT-treated mice, macrophages were nearly undetectable, while the proportion of monocytes was markedly increased. In contrast, the proportion of neutrophils remained largely unchanged (Fig. S5C). For lymphoid cells, the changes in cell proportions within the pleural cavity were similar to those observed in the tumor. The proportions of T cells and NK cells were increased, while the proportion of B cells was reduced (Fig. S5D). Given the observed increase in T-cell proportions and the reduced tumor growth following macrophage depletion, we further examined the proportion of cytotoxic $CD8^+$ T cells. We found that the depletion of pleural cavity macrophages led to an upregulation of cytotoxic T cells in both the tumor and the pleural cavity (Fig. S5E and S5F). Based on the above analysis of immune cells in the tumor and pleural cavity, we propose that depletion of pleural cavity macrophages promotes the accumulation of cytotoxic T cells, thereby enhancing anti-tumor immune responses and contributing to the suppression of tumor growth.

This study effectively utilized a dual recombinase-mediated genetic system to trace pleural cavity macrophages in a B16F10 melanoma lung metastasis mouse model. Fate mapping demonstrated that these cavity macrophages significantly infiltrate the tumor, constituting a substantial portion of its macrophage population. Crucially, the genetic ablation or knockout of *Gata6* in these macrophages led to a decreased tumor burden and improved survival rates. These findings underscore the pivotal role of cavity macrophages in tumor growth and metastasis dynamics, suggesting that targeting these cells may represent a promising therapeutic strategy for tackling tumor progression. The cellular dynamics observed in our work indicate that the molecular mechanisms driving the migration and functional activities of cavity macrophages merit further investigation, potentially revealing new therapeutic targets *per se*.

## Supplementary data

Supplementary data is available at *Protein & Cell* online at https://doi.org/10.1093/procel/pwaf078.

## Footnotes

We thank Shanghai Model Organisms Center, Inc. for mouse generation. We thank Dr Hongkui Zeng for kindly providing reporter mice and Dr Yi Zeng for kindly providing the *Gata6-flox* mouse (jax008196). We thank members of the animal facility and cell platform in CEMCS for animal husbandry and assistance in flow cytometry and microscope.

The authors declare no conflict of interest.

This work was supported by the National Key Research & Development Program of China (2024YFA1803302, 2023YFA1801300, 2023YFA1800700), the National Science Foundation of China (82088101), the Youth Innovation Promotion Association CAS, the Shanghai Pilot Program for Basic Research—CAS, Shanghai Branch (JCYJ-SHFY-2021-0), the Research Funds of Hangzhou Institute for Advanced Study (2025HIAS-ZL005), the Shanghai Municipal Science and Technology Major Project, the Innovative Research Team of High-Level Local Universities in Shanghai, and the New Cornerstone Science Foundation through the New Cornerstone Investigator Program and the XPLORER PRIZE.

Z.Z. performed the investigation, conducted formal analysis, curated the data, and wrote the original draft of the manuscript. H.J. and Z.L. contributed to formal analysis and visualization. M.S., M.Z., W.P., and J.L. provided experimental materials. X.L., D.M., and Q.S. co-supervised the study and provided funding for the study. B.Z. conceptualized the study, reviewed and edited the manuscript, and supervised the research. All authors approve the publication of this manuscript.

The data supporting the findings of this study are available from the corresponding author upon reasonable request.

All mouse experiments were approved by the Institutional Animal Care and Use Committee (IACUC) of the Center for Excellence in Molecular Cell Science, Chinese Academy of Sciences. All animal experiments were strictly performed within the committee's guidelines.

## References

Buechler MB, Kim KW, Onufer EJ et al.A stromal niche defined by expression of the transcription factor WT1 mediates programming and homeostasis of cavity-resident macrophages. *Immunity* 2019;**51**:119–130.e5.

Chow A, Schad S, Green MD et al.Tim-4$^+$ cavity-resident macrophages impair anti-tumor CD8$^+$ T cell immunity. *Cancer Cell* 2021;**39**:973–988.e9.

Deniset JF, Belke D, Lee WY et al.*Gata6*$^+$ pericardial cavity macrophages relocate to the injured heart and prevent cardiac fibrosis. *Immunity* 2019;**51**:131–140.e5.

Donnenberg AD, Luketich JD, Dhupar R et al.Treatment of malignant pleural effusions: the case for localized immunotherapy. *J Immunother Cancer* 2019;**7**:110.

Jin H, Liu K, Huang X et al.Genetic lineage tracing of pericardial cavity macrophages in the injured heart. *Circ Res* 2022;**130**:1682–1697.

Jin H, Liu K, Tang J, et al.Genetic fate-mapping reveals surface accumulation but not deep organ invasion of pleural and peritoneal cavity macrophages following injury. *Nat Commun* 2021;**12**:2863.

Madisen L, Zwingman TA, Sunkin SM et al.A robust and high-throughput Cre reporting and characterization system for the whole mouse brain. *Nat Neurosci* 2010;**13**:133–140.

Morano WF, Aggarwal A, Love P et al.Intraperitoneal immunotherapy: historical perspectives and modern therapy. *Cancer Gene Ther* 2016;**23**:373–381.

Porcel JM, Gasol A, Bielsa S et al.Clinical features and survival of lung cancer patients with pleural effusions. *Respirology* 2015;**20**:654–659.

Rosas M, Davies LC, Giles PJ et al.The transcription factor *Gata6* links tissue macrophage phenotype and proliferative renewal. *Science* 2014;**344**:645–648.

Sodhi CP, Li J, Duncan SA. Generation of mice harbouring a conditional loss-of-function allele of *Gata6*. *BMC Dev Biol* 2006;**6**:19.

Wang J, Kubes P. A reservoir of mature cavity macrophages that can rapidly invade visceral organs to affect tissue repair. *Cell* 2016;**165**:668–678.